Chapter 5

Dynamic and static tribological properties of micropatterned DLC under different humidities

5.1 Introduction

Sliding friction occurs in a large number of technological processes and in everyday life [7]. Developing a deep understanding of its mechanisms is important in our search for ways to control or minimize friction and wear between sliding surfaces. In this Chapter we focus on sliding friction when one of the two surfaces has a hydrogenated DLC coating. In order to define the precise regions where the DLC coating makes mechanical contact, we micropatterned our DLC-coated samples with cylindrical mesas, similar to the ones discussed in Chapter 4. In Chapter 5, we concentrate on the dependence of friction on two parameters, namely the sliding velocity and the humidity of the air.

Sliding friction is usually considered to be independent of velocity. Charles Coulomb (1736-1806) postulated this in his law of dry friction, stating that "when two solid bodies are in contact, the force required to produce sliding between them is proportional to the normal force acting in the plane of contacts" [37]. In mathematical terms,

$$F_f = \mu_d F_N, \tag{5.1}$$

where F_f is friction force, F_N is the normal load and μ_d is the coefficient of sliding, or dynamic friction. Indeed, in this so-called Amontons-Coulomb law [77], F_f does not depend on sliding velocity. However, over the past decades, careful studies demonstrated that friction does depend on sliding velocity and that this law oversimplifies the interaction between the sliding objects [31, 32, 38, 39]. Both on the nano- and on the macroscale, certain materials exhibit a decrease of the coefficient of friction with increasing velocity [6,34,35]. Other materials, on the other hand, show an increase [31-34], while there are also materials for which the friction coefficient varies non-monotonically with velocity [32,35,40]. A near velocity-independence was demonstrated for an AFM tip sliding over amorphous carbon, diamond and HOPG surfaces [41]. The differences in behavior derive from different material properties, in particular from differences in the structure and composition of the surfaces and their interaction with the environment. Effects that play a role are for example the aging of contacts [46,42,44], plastic and elastic shear of asperities [43,45,47], hydrodynamic effects such as the viscous behavior of

adsorbed water necks and lubrication layers [14,23,40,48], and tribochemical effects [e.g. 35]. It has also been shown that even at room temperature, capillary condensation of adsorbed water between e.g. a metal tip and a graphite surface can lead to the formation of ice, which significantly increases the friction force between them at low velocities [24, 25].

Friction phenomena on DLC are also complex. First of all, they should be always described as a three-body contact problem. A third-body is not only a layer of particle debris and other wear products created during sliding between the contacting surfaces, but it can also be adsorbed vapor [1, 63]. Depending on the surface and interfacial energies, capillary bridges can be created between surfaces that are either in contact or close to contact [3-6, 22]. Viscous shear of capillaries can dramatically alter the friction and wear properties both on the nano- [6, 13, 14, 23] and on the macroscale [8-12]. Depending on hydrophilicity of the surfaces and their roughness, the friction force can display either increasing or decreasing behavior as a function of e.g. sliding speed and relative humidity [16-21]. However, at present there is still much controversy on the general effects of velocity and relative humidity on friction properties of DLC coatings.

In this study, we consider how particle debris formed during the run-in period plays a major role in the lubrication of the interface between a sliding object and the DLC surface. In this context, we also take into account the influence of capillary forces acting between them [2, 15]. Tribochemical reactions on the DLC might affect the friction coefficient differently under different atmospheric conditions [11, 14, 26-28]. Here, we discuss experiments on the sliding-velocity-dependence and the aging of contacts at different levels of relative humidity on micropatterned samples with a-C:H DLC coatings.

5.2 Experimental

The experimental details were thoroughly discussed already in Chapter 4. In summary, Dylyn a-C:H DLC coatings were applied by means of magnetron sputter deposition on pre-polished SiSiC substrates. On the coated surfaces, we measured a contact angle for water of 85°, so our particular DLC coating should be considered partially hydrophobic.

Our friction measurements were performed with a Bruker Universal Mechanical Tester (UMT), described in detail in Chapter 4. The role of the counter-surface was played by a 2-inch diameter silicon wafer, 250 μm thick. The weight of each wafer of approximately 12 mN served as the normal force in the sliding experiments. The contact angle of water with the wafer, covered with its native oxide SiO_2, was measured to be 36° (strongly hydrophilic). The wafers were used directly from the supplier [76], where they had been pre-packed under cleanroom conditions, so that no further cleaning was needed, prior to the experiments.

In our experiments, the relative humidity (RH) was measured close to the substrate position with a hygrometer, Vaisala HM40 [78]. The RH value could be varied between 1.5 and 90% (at room temperature, $22°C$) by means of a flow of a controlled mixture of dry nitrogen and humid air through the microscope chamber.

5.3 Experimental results

Figure 5.1 shows the result of the measurement of the dependence of the coefficient of friction on sliding velocity. Prior to the test, the DLC-coated substrate was 'run-in' against a silicon wafer, until the COF had settled at a low value of 0.08 (described in detail in Chapter 4). The measurements were performed under three different levels of RH: 1.7% (dry), 35% ('regular') and 88% (humid). The sliding velocity of the silicon wafer with respect to the DLC-coated substrate was gradually varied over a wide range, from 200 nm/sec to 1 mm/sec (1 $\mu m/sec \div 2\ mm/sec$ in the case of $RH = 1.7\%$). The maximum driving velocity of 2 mm/sec of the UMT was set by its limited stroke length. The minimum driving velocity was limited by the minimal step of the rotary drive, and was equal to 100 nm/sec. For each set of measurements over a range of velocities at the given RH a new silicon

wafer was used. For each combination of humidity and velocity, three measurements were performed along the same stroke direction and the average value of COF was calculated. Thus, a typical error margin for each data point is about 2% of its average value. The COF-values determined at dry conditions ($RH = 1.7\%$) show a nearly logarithmic dependence on velocity over the full velocity range. At higher RH levels, the low-velocity data points deviate from the logarithmic behavior (marked with ovals in Fig. 2.1). For $RH = 35\%$, a minor deviation is observed in the range of $200\,nm/sec$ to $5\,\mu m/sec$, while the COF is almost constant at $RH = 88\%$ between $200\,nm/sec$ and $20\,\mu m/sec$. A logarithmic increase of the friction coefficient with the sliding velocity is in qualitative agreement with friction studies between partially hydrophobic surfaces and the hydrophilic native oxide of silicon [6, 33].

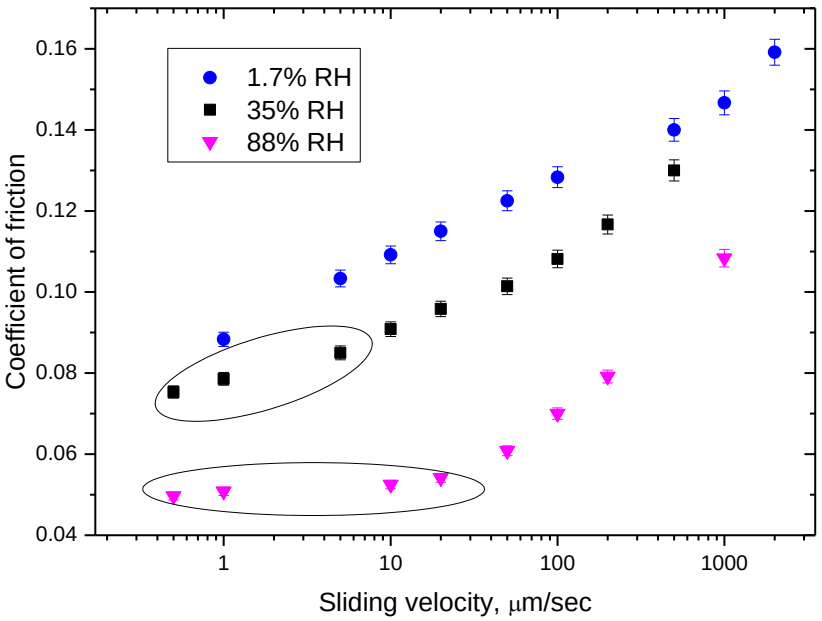

Figure 5.1. Dynamic coefficient of friction as a function of sliding velocity between silicon wafers and a DLC-coated SiSiC substrate. Measurements were carried out at three different humidity levels, $RH = 1.7\%$, 35% and 88%. The normal load of $12\,mN$ was fixed by the weight of the wafers.

As Figure 2.1 shows, the frictional behavior of the DLC/SiO_2 interface appears to be rather sensitive to the RH level. To explore this in more detail, we carried out a series of measurements at certain constant velocities as a function of RH. Figure 5.2 shows the dynamic COF versus RH at 1 $\mu m/sec$, 10 $\mu m/sec$ and 100 $\mu m/sec$. For each velocity, a series of measurements was performed while we gradually made RH increase from 2% to 90% and then made it reduce back to 35%. Each data point in Figure 5.2 represents the average value of three consecutive measurements at the same combination of velocity and RH level. No hysteresis was observed between the measured values of the friction coefficient upon the gradual increase or decrease of RH. The corresponding curves are plotted on a logarithmic RH-scale in order to emphasize the 'abruptness' of the reduction in COF at higher RH-values for all three velocities. This occurs around $RH = 55\%$, independent of the velocity. For each velocity, the COF is high and almost constant at RH levels below this value.

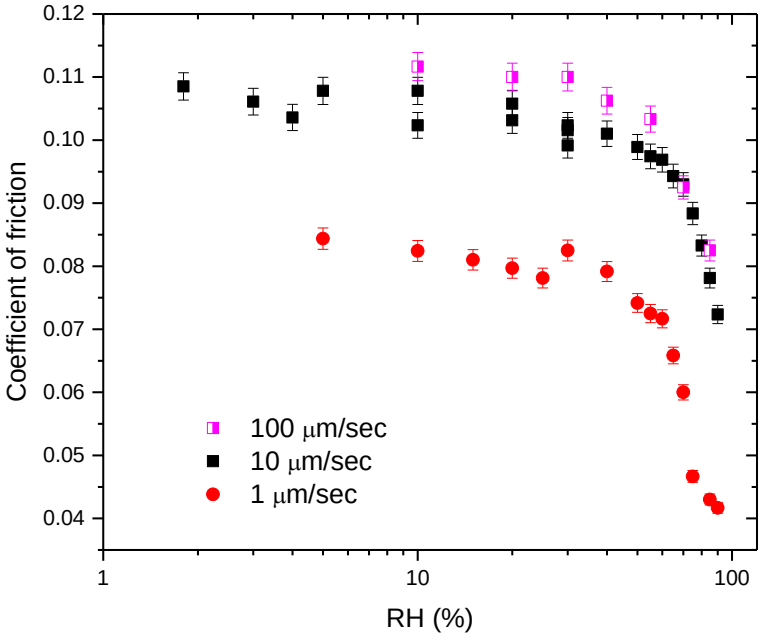

Figure 5.2. Dependence of the dynamic COF between silicon wafers and a DLC-coated SiSiC substrate on the relative humidity RH at three different sliding velocities.

Another sensitive quantity that we can determine in our experiments is the static friction coefficient μ_s, which is defined as the ratio between the minimum tangential force $F_s = \mu_s F_N$ one needs to apply in order to initiate the relative sliding of two objects and the normal force F_N between them. Usually $\mu_s > \mu_d$ (Fig. 5.3). For various materials μ_s increases quasi-logarithmically with the 'age' of the static contact τ prior to sliding $\mu_s(\tau) \approx \mu_s^0 + \beta_s \ln(\tau)$, where β_s is a coefficient specific for contacting materials and temperature, and μ_s^0 is the static threshhold base value [43].

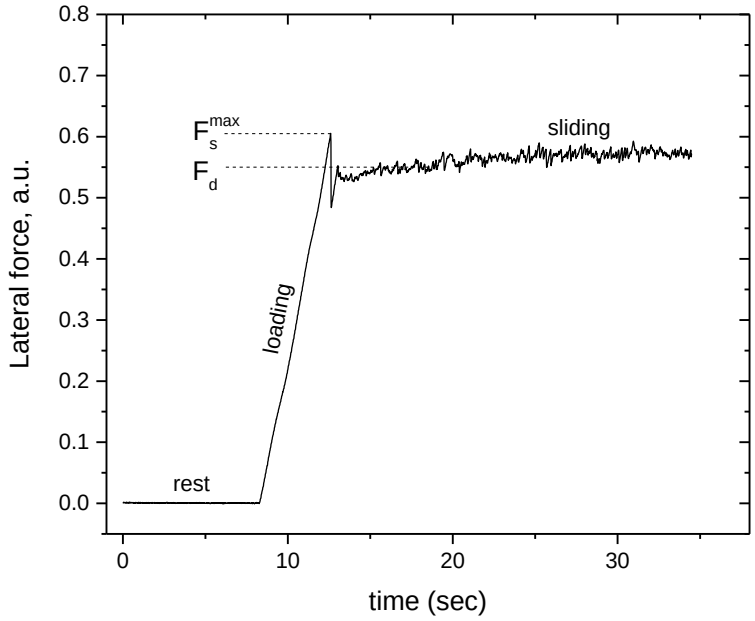

Figure 5.3. An example of the lateral force between two solid surfaces, in this case a Si wafer sliding over a DLC surface (Chapter 4), as a function of time at the beginning of a sliding experiment. After an initial period, during which no lateral force is exerted on the contact (rest), a lateral force is accumulated (loading). When this exceeds the static threshold level $F_s^{max} = \mu_s F_n$, sliding starts, after which the lateral force reduces to the dynamic value of $F_d = \mu_d F_n$. Note, that in the example shown here, the system goes through one additional stick-slip cycle before truly steady sliding sets in.

Figure 5.4 represents the dependence of the static coefficient of friction μ_s on contact aging time, i.e. the time spent by the silicon wafer in rest on the micropatterned DLC substrate, prior to sliding. These measurements of the static

COF were carried out at three different RH levels, 0.66%, 35% and 90%. During the dwell time, the pusher of the UMT always remained engaged with the silicon wafer (arrested contact), while the lateral force was measured to decrease slowly in time due to relaxation at the interface, before reaching a certain constant equilibrium value [e.g. 47]. After this dwell time, the pusher was put into motion at a velocity of 20 $\mu m/sec$, which made the lateral force increase at a rate of 1.5 mN/sec to the static lateral force maximum F_s^{max}. At this point the silicon wafer would be set into motion, which would make the lateral force reduce to the dynamic friction force level F_d. For each μ_s value in Fig. 5.4, we used the average of three measurements of F_s^{max}.

Over the explored range of aging times $1 \leq \tau \leq 500\ s$, in Figure 5.4, the data at the lower two RH-values show a weak logarithmic dependence of the static COF. Whereas μ_s decreases under dry conditions, for $RH = 0.66\%$ (the fit is for $\mu_s = 0.11 - 2.91 \times 10^{-4} ln(\tau)$, with τ expressed in seconds), it increases at $RH = 35\%$ (the fit is for $\mu_s = 0.10 + 7.76 \times 10^{-4} ln(\tau)$). Under very humid conditions (RH = 90%), μ_s is found to increase logarithmically with the aging time only above approximately 20 sec (marked as II in Fig. 5.4). For shorter aging times (below 20 sec, marked as I), we find only a very modest slope of the logarithmic increase of μ_s.

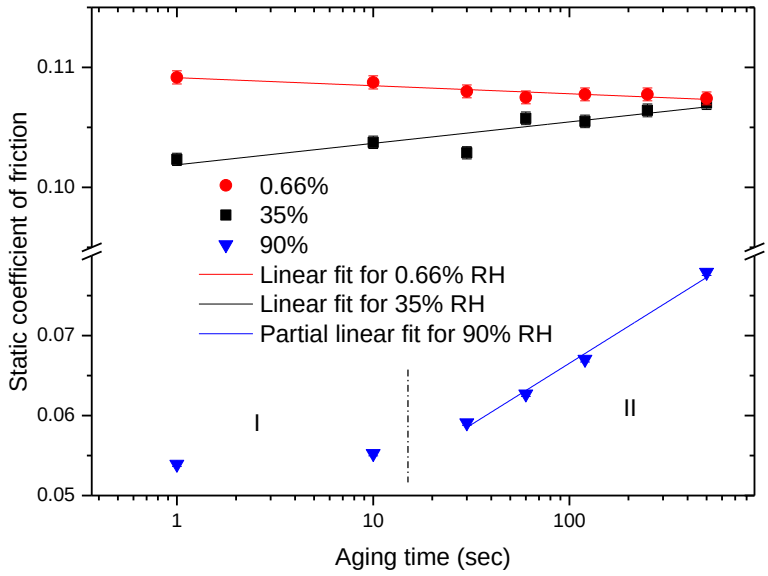

Figure 5.4. Dependence of static friction coefficient on contact aging time τ at three different values of RH, for silicon wafers on DLC-coated SiSiC substrates. The normal force of $12\ mN$ *was set by the weight of the wafers. The static force maximum was measured at a rate of lateral force increase of* $1.5\ mN/s$.

5.4 Discussion

Opposite to our observations, many other studies have found an increase in friction of a-C:H DLC with increasing humidity [e.g. 18, 52, 58, 59, 75]. Only a modest number of papers report a decrease, similar to our findings for hydrogenated DLC films [81, 64, 57]. Most studies agree that under dry conditions a-C:H films remain largely inert [27]. The presence of hydrogen leads to extremely weak adhesion [29, 30] in interfaces that involve hydrogenated DLC films, so that extremely low friction coefficients can be achieved [82]. Hydrogen added to the DLC film can saturate the dangling σ-bonds of carbon atoms [18]. Similarly, it can suppress the number of C=C double bonds (particularly π-π* interactions). However, when the DLC-lubricated contacts are exposed to high humidity levels, in many cases the friction properties exhibit significant changes. Often, for $RH > 40\%$, the friction coefficient and the wear rate are found to rapidly grow. Most of these observations can be associated with tribochemical oxidation of DLC

films during the friction process at elevated humidity. Based on X-ray photoelectron spectroscopy analysis (XPS), Li et al. [58] proposed a model to explain the transformation of initially chemically inert hydrogenated DLC into an oxygen-containing surface. They suggest that the increased adsorption rate of water molecules on the DLC surface at high humidities increases the probability of water chemisorption at the surface sites were C-H bonds are mechanically broken by the high shear stresses that develop locally during sliding. As a consequence, C-OH and C-O groups may be formed. Further breaking of C-H bonds will provide the electrons required to form C=O on the DLC surface, which leads to the accumulation of a thin oxide layer on the contacting elements. In turn, this leads to a rapid increase of the friction coefficient. On top of this, water can adsorb on the oxide surface, introducing strong dipole interactions that increase the adhesive forces between the sliding surfaces [28].

In our study, the DLC coatings show the highest dynamic (sliding) friction coefficient $\mu_d = 0.11$ at high velocities under dry conditions ($RH = 1\%$) and reach the lowest value $\mu_d = 0.04$ at low velocities under humid conditions ($RH = 90\%$). A significant lowering of the friction coefficient is observed at $RH = 55\% \pm 4\%$ (Fig. 5.2). In our study, the measurements carried out at different RH values and at different velocities were completely reversible, i.e. the accompanying changes in the COF were instantaneous and free of hysteresis. This strongly suggests that in our case the interaction of the coating with water vapor has a purely *physical* adsorption character, rather than involving water-induced chemical changes in the coating that would be necessarily accompanied with an intrinsic timescale and a hysteretic tendency. Even though the chemical composition of our hydrogenated DLC coatings is very similar to that of DLC coatings for which friction measurements have been reported before in the literature [17, 18, 27, 57], our observations show systematic differences. These must find their origin in other differences in our experimental setting, in particular in our special flat-disk-on-rough-mesas contact geometry, and in our combination of modest sliding velocities and a relatively low normal load. By contrast, most of experiments in this field are conducted with balls and pins sliding over DLC-coated substrates under conditions that are relevant for the automotive industry: high normal loads and high velocities. Also the typical sliding distances in most experiments are relatively large. Hence the surface of the sliding ball or pin may be in contact at each stage of

the sliding process not only with parts of the transfer layer [21 and 83], but also with fresh parts of the DLC surface, which could make the interface sensitive to the chemical, e.g. oxidation state of the DLC surface.

We used micropatterned DLC substrates in combination with flat silicon wafers as the counter-surface. Similar to other studies, we find a clear correlation between the presence of third-body C-based particles on the DLC film, and the reduction of the dynamic friction coefficients [e.g. 60]. As we demonstrated with our Raman spectroscopy measurements (Chapter 4), these particles (and some asperities) have a short-range disordered microstructure, similar to that of disordered graphite. Our flat-on-rough-mesa interface geometry guarantees that the highest protrusions on the DLC-surface, which are either asperities on the DLC-coating itself or high-lying third-body particles, remain in continuous direct mechanical contact with the flat silicon counter-surface, more or less independently of the sliding velocity and the humidity. This is very different from the more common rough-on-rough situation, in which each local contact has a typical 'lifetime' that is determined by the ratio between its size and the sliding velocity. In our situation, the contacts are 'fixed' and their lifetime is practically infinite! Obviously, this may have distinct implications for the dependence of the friction force on velocity and on humidity.

First, at the beginning of sliding, the decomposed loose particles reduce friction due to weak van der Waals interaction, thus low adhesion, between their hydrogen terminated surfaces. Here we assume that a water film is adsorbed on the hydrophilic native silicon oxide surface and that this water film reduces friction by keeping the surfaces out of direct mechanical contact. As sliding proceeds, more and more C-H bonds on the particles rupture. This happens under the high contact pressure, the high shear stresses and the generation of thermal energy during sliding. This leads to the thermally activated release of H atoms and, hence, the rapid decrease of the total hydrogen content in each particle and its (partial) graphitization [57, 63]. As a result, the particles and other sp^2-modified areas will develop micro-ordered low-energy surfaces [62]. Whereas these surfaces can be extremely slippery, the dangling bonds (free σ-bonds) at the edges of the newly created sp^2 clusters can engage in new bonds that lead to pinning of the clusters and pinning of the water that is sliding over them. When the humidity is not too low, the dangling bonds are re-passivated with H-atoms and OH-groups,

originating from water molecules that dissociate at the reactive edges [79, 80]. At high enough humidity, water will form an adsorbed layer that separates the contacting surfaces and thus acts as a lubricant [49, 61]. A similar water lubrication action is associated with non-hydrogenated DLC [51, 64]. We also cannot exclude the possible oxidation of the DLC film at higher humidity, as was reported in [58]. On the other hand, if an oxide layer was formed on the DLC surface, this should result in a new run-in phase of the DLC, thus increase of the friction coefficient [17]. Our observations do not provide strong arguments in favor of the formation of an oxide layer on our DLC layers, because the friction coefficients measured in this study were completely reversible with respect to changes in RH.

In addition to the lubrication of sp^2 clusters, water can also play other roles. Firstly, pristine hydrogenated DLC has partially hydrophobic properties and its friction behavior is almost independent of RH [13]. At the same time, the first monolayer of water molecules that are strongly bonded to the silicon counter-surface are not likely to be pressed out of the contact [23, 33, 34]. Instead, the water film will be sheared across the DLC surface during sliding, again keeping the surfaces out of direct mechanical contact. Secondly, the graphitization of particles and the contacting asperities on the DLC coating leads to the existence of hydrophilic 'islands'. Therefore, we expect these crucial regions on the DLC side to engage in capillary effects. The viscoelasticity of the confined water in the capillary bridges between these regions and the silicon surface may affect both the dynamic and the static friction behavior [6, 13, 32, 33]. We can only conclude that, depending on the history of the sliding contact and the conditions under which a sliding experiment is conducted, each individual experiment may display its own combination of lubricating and pinning properties of water. An artist impression that captures some of this complexity of the interface between a rough DLC substrate and an oxide-covered, smooth silicon wafer, in the presence of wear particles and in a humid atmosphere, is presented in Fig. 5.5.

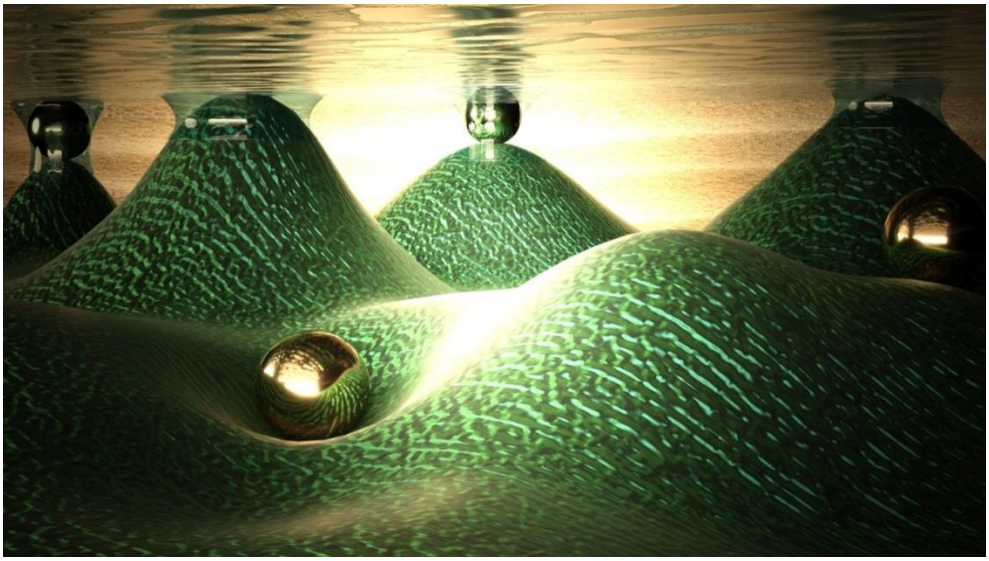

Figure 5.5. Artist impression of the interface between a rough DLC coating (bottom surface) and a smooth, oxide-covered silicon wafer (top surface) in a humid atmosphere. For simplicity, the third-body particles that have been formed during the run-in phase of the contact, are presented as spherical objects. We distinguish two types of contacts, namely direct contacts between the DLC and the wafer and contacts via one of the particles. Both types are decorated by capillary water bridges.

In Fig. 5.2 we showed how the dynamic friction coefficient μ_d varies with humidity at three fixed velocities. For example, at a velocity of 1 $\mu m/sec$, μ_d has values as low as 0.05 at $RH = 80\%$ and as high as 0.09 at $RH = 1.7\%$. The corresponding friction force curves (Fig. 5.6), also show a qualitative difference in the sliding behavior. We observe that at the lower humidity the friction exhibits much stronger variations than at higher humidities. At higher RH, a modest, stick-slip-like periodicity is visible. Also the initial sliding behavior differs. The curves for low- and medium-RH in Fig. 5.6 start almost at the same lateral force of 0.95 mN. This is mainly due to the minor difference between the static coefficient of friction at low-RH and medium-RH (Fig. 5.2). Moreover, the waiting time prior to the actual pushing and measurement in the both cases was longer than 300 sec. Such waiting time is necessary for stabilization of RH in the test chamber. It is only after sliding over a distance in the order of 10 μm, that the humidity-dependent differences are fully established.

In an attempt to explain the curves in Fig. 5.6, we first concentrate on the low-RH data. The noise on the lateral force at $RH = 1.7\%$ suggests that the contact geometry is not completely stationary. This could mean that the third bodies are translated over the DLC surface under the influence of the shear forces that they experience [33, 42 and 47]. It is not surprising that this situation leads to stronger energy dissipation, hence higher friction levels [32]. The absence of this effect at somewhat higher RH-levels could be due to the presence of capillary bridges that connect these particles to the DLC substrate, in spite of the fact that neither the substrate nor the particles are fully hydrophilic. As we have already seen in Fig. 2.2, almost independently of the sliding velocity, water starts to significantly lubricate the surface at an RH-level around 55%. This is in good agreement with the known adsorption kinetics of water on graphitic materials [49, 50 and 84]. The buildup of water between the DLC (third bodies and asperities) and the silicon would then explain the dramatic lowering of the friction between $RH = 35\%$ and 80%.

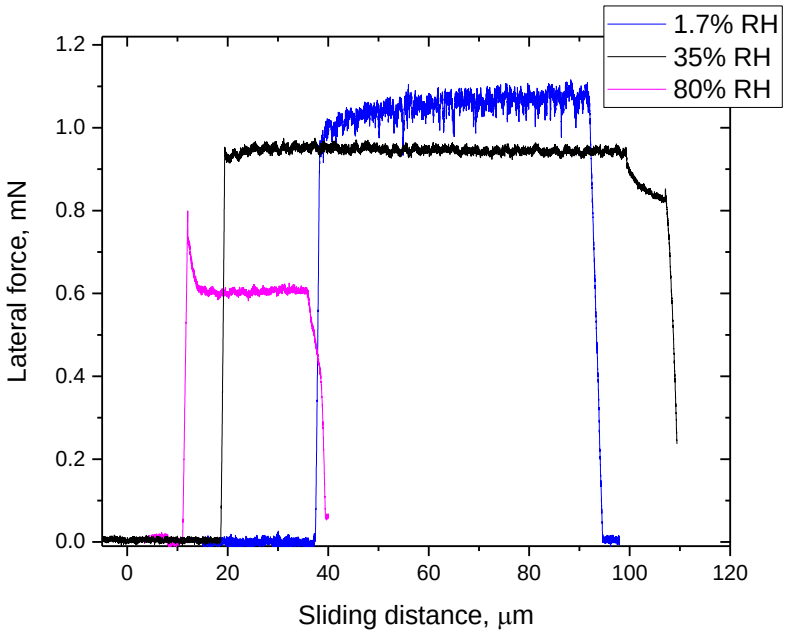

Figure 5.6. Lateral forces measured between a DLC-coated SiSiC substrate and a silicon wafer in three sliding traces at a fixed velocity of $1\ \mu m/sec$ *at RH-values of* 1.7%, 35% *and* 80%. *The normal load was* $12\ mN$ *in all three cases. The horizontal axis indicates the lateral position of the push bar; the precise starting point of the actual sliding motion of the silicon wafer was different for every curve.*

We now revisit the measured dynamic (Fig. 5.1) and static (Fig 5.4) friction coefficients in an attempt to make a direct comparison between the two. A natural way in which the two are often related is via the average lifetime of microcontacts, which equals the ratio between the average diameter of microcontacts and the sliding velocity [47]. For those phenomena that are a function of contact time, such as capillary condensation over existing contacts and near-contacts or elastic and plastic creep, this average contact lifetime then plays a similar role as the waiting time does for static friction. With respect to the microcontact lifetimes, the situation in our experiments seems fundamentally different. The lifetime of our microcontacts is extremely long as a direct consequence of the geometry of our experiments, in which one of the two contacting bodies, the silicon wafer, is nearly perfectly flat. However, when the third bodies on the DLC side can move, as we

have argued for the low-RH data in Fig. 5.6, the arrangement of microcontacts is no longer stationary and a new type of lifetime is introduced.

In our experiments, the details of the measurement technique introduce a direct link between static and dynamic friction measurements. The driver motor that is used in our UMT to generate the sliding motion is a linear stepper motor. On the microscale, its motion is not continuous but is composed of periodic translations, the minimum step size being $100\,nm$, separated by stationary intervals. Therefore, we can interpret our dynamic friction measurements as measurements of the static friction force after a short waiting time. This allows us to combine the data in the two graphs of Figs. 5.1 and 5.4 into a single one, in which we can express the control parameter either in terms of the effective sliding velocity or the effective waiting time. The result of this combination is shown in Fig. 5.7.

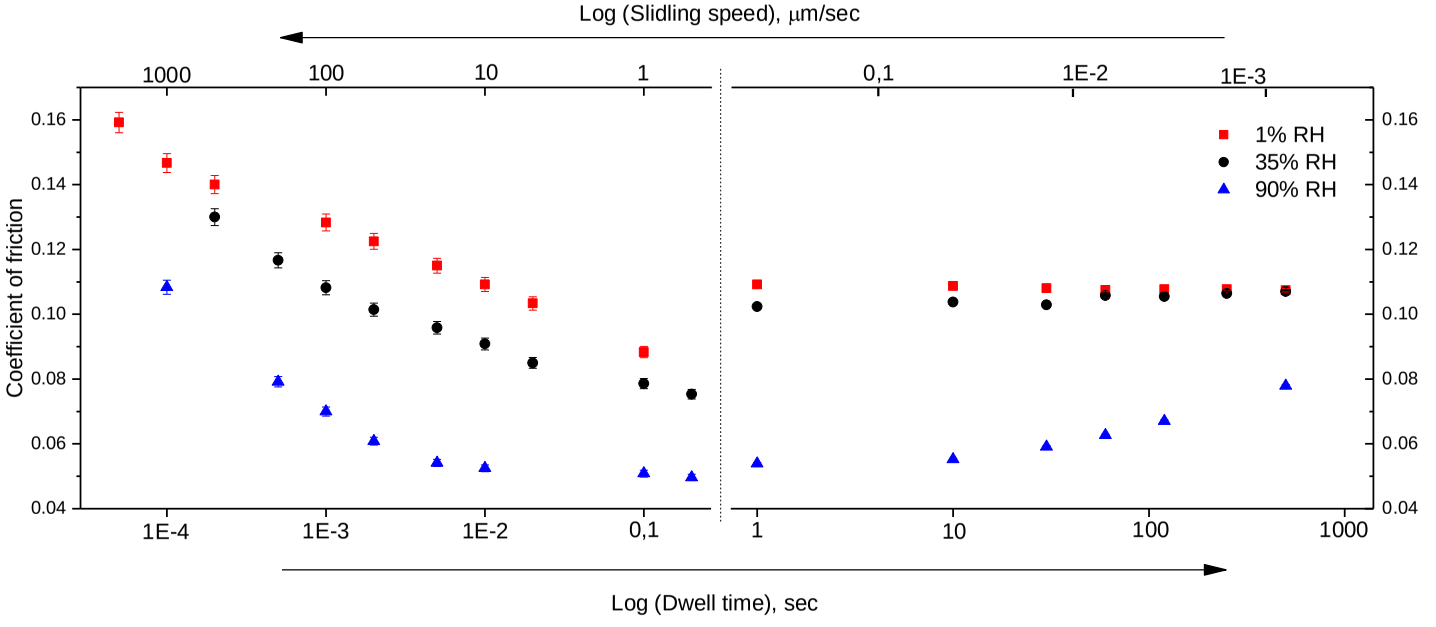

Figure 5.7. Combined representation of measured coefficients of friction, expressed as a function of sliding velocity and waiting time, based on the μ_d-data from Fig. 5.1 and the μ_s-data from Fig. 5.4. The vertical dashed line points where the data from Fig. 5.1 and Fig. 5.4 merge.

Figure 5.7 shows that at all three RH levels, the friction force decreases with increasing waiting time (or decreasing sliding velocity) up to a transition point around a waiting time of 1 sec. For the lower two humidities of $RH = 1\%$ and 35%, μ_d remains nearly constant for all waiting times longer than 1 sec. For the higher humidity of 90%, we find that longer waiting times lead to increasing μ_d values. As already discussed in relation to the friction curves in Fig. 5.6, we interpret the low- and medium-RH data in terms of the sliding-induced translation of third bodies over the DLC substrate. In this interpretation, capillary condensation serves to attach the third bodies to the DLC, which progressively fails at shorter waiting times and lower humidities [6, 55, 65-67]. The factor 35 between the lower two RH-values corresponds with the roughly equally large ratio between the timescales of the friction data in Fig. 5.7 for 1% and 35% humidity, completely in support of this scenario. A similar scaling can only account for part of the difference between the 90% data and those at the lower two humidities of 35% and 1%. What this scenario also fails to explain is the marked increase of friction at $RH = 90\%$ for longer waiting times.

In wet environments, such as $RH = 90\%$, water menisci nucleate from water vapor between the DLC substrate, with its asperities and nanoscale third-body particles, and the silicon wafer (Fig. 5.5). This nucleation process should occur on a very short time. The typical timescale for the condensation of one layer of water molecules at room temperature and at a humidity of $RH = 65\%$ is an estimate of 25 μs [6]. Therefore, we should expect that only a limited number of DLC-silicon contacts is decorated with a condensate, when the waiting time is short [68]. The geometry and size of each fully established capillary neck is dictated by the Kelvin relation [70]. When the waiting time is increased, the number of capillary bridges and, hence, the total water-decorated area will increase. A detailed discussion of the kinetics of the formation of capillary bridges can be found in e.g. [55, 68]. Liquid bridges introduce significant adhesion and thereby reduce the mobility of the third-body particles between the sliding surfaces in humid air. When the sliding velocity is increased, the capillary bridges will be increasingly sheared and even fully developed bridges may not remain intact. The shearing of the capillary bridges may be accompanied by the repeated breaking or melting of crystallized water layers inside the capillaries, as ice is known to form at low sliding speeds, even at room temperature [24]. When a capillary bridge is destroyed, a new one

cannot be formed immediately to replace it, because of the nucleation barrier that is involved in the start of a new capillary bridge [6, 71]. Around a certain critical sliding velocity v_c, the effective size of the sheared capillaries is optimally reduced by the sliding motion for them to minimize the viscous contribution to the friction force, while maintaining the beneficial effect of the water in binding the third-body particles to the DLC. This results in a plateau of low friction around $v_c = 1\ \mu m/sec$ at $RH = 90\%$ and a narrow minimum at the same velocity for $RH = 35\%$ and $RH = 1\%$, as shown at Fig. 5.7.

Finally, we note that the friction at the nanoscale contacts could be affected by thermal activation, similar to what has been reported for the low-friction sliding of FFM tips over surfaces [56, 72,74], and what was one of our motivations for manufacturing the nanopillar structures of Chapter 3. At sufficiently low velocities, thermal fluctuations can assist the tip in overcoming the energy barriers that separates it from the neighboring energy minima in its interaction with the surface over which it is sliding. This phenomenon is called thermolubricity. At higher sliding velocities, less time is available for this role of thermal fluctuations, which renders this effect less successful and makes the friction force an increasing function of velocity. All experiments in this chapter were performed at room temperature. More experiments are currently underway to explore the influence of temperature on friction properties of the investigated DLC-silicon interface. We expect that elevated temperatures can strongly influence the friction coefficient not only through thermolubricity, but possibly also via thermally activated water desorption from the contact areas [14] and thermally activated rupture of contacts due to their spontaneous unbinding [53].

5.5 Conclusions

We have shown that the friction properties of hydrogenated DLC coatings in dry and humid environments are surprisingly different from common tribological behavior of this type of coatings. We ascribe this difference largely to the unusual geometry of our experiment; in our measurements, most microcontacts do not leave the actual sliding interface, which is due to the combination of the micropatterned DLC substrate and the flat, silicon counter-surface. This geometry accelerates the run-in process and assists the DLC-induced lubrication. In the first

part of this chapter, we have shown that the run-in leads to two types of modification of the DLC surface, namely the accumulation of carbon-based third bodies and a bonding reconfiguration of these wear particles and of the asperities of the DLC; both exhibit a change from sp^3 to sp^2 bonding character, i.e. from diamond-like to graphite-like. Here we have further shown that water adsorbed from a mildly humid environment can play a lubricating role for the graphitized DLC clusters at low sliding velocities, which we associate with capillary condensation of water between them and their DLC substrate. At high humidities, friction is lowered even further, suggesting a hydrodynamic contribution, i.e. water acting directly as a lubricant, for example due to the formation of capillary bridges between the oxidized silicon surface and the surfaces of the graphitized DLC particles and DLC asperities.

5.6 Bibliography

1. Auroux, A. Calorimetry and thermal methods in catalysis. *Springer-Verlag*, Berlin (2013)
2. Dörmann, M. & Schmid, H.-J. Simulation of Capillary Bridges between Particles. *Procedia Engineering* **102**, pp. 14-23 (2015)
3. van Honschoten, T. *et al*. The profile of a capillary liquid bridge between solid surfaces. *American Journal of Physics* **78**, pp. 277-286 (2010)
4. Landau, L.D. and Lifschitz, E.M. Fluid Mechanics, 2nd ed. Butterworth Heineman, Oxford (1971)
5. Petkov, P. & Radoev, B. Statics and dynamics of capillary bridges. *Colloids and Surfaces A: Physicochemical and Engineering Aspects* **460**, pp. 18-27 (2014)
6. Riedo, E., Lévy, F. & Brune, H. Kinetics of Capillary Condensation in Nanoscopic Sliding Friction. *Physical Review Letters* **88**, 185505 (2002)
7. Persson, B. & Spencer, N. Sliding Friction: Physical Principles and Applications. *Physics Today* **52**, pp. 66-68 (1999)
8. Lancaster, J.K. A review of the influence of environmental humidity and water on friction, lubrication and wear. *Tribology International* **23**, pp. 371-389 (1990)
9. Klaffke, D. On the repeatability of friction and wear results and on the influence of humidity in oscillating sliding tests of steel-steel pairings. *Wear* **189**, pp. 117-121 (1995)
10. Ronkainen, H. *et al*. Friction and wear properties in dry, water- and oil-lubricated DLC against alumina and DLC against steel contacts. *Wear* **222**, pp. 120-128 (1998)
11. Eriksson, A. *et al*. A study of the influence of humidity on the friction and squeal generation of automotive brake pads. *Journal of Automobile Engineering* **215**, pp. 329-342 (2001)
12. Lee, W. *et al*. The influence of humidity on the sliding friction of brake friction material. *Wear* **302**, pp. 1397-1403 (2013)
13. Lee, M., Kim, B., Kim, J. & Jhe, W. Noncontact friction via capillary shear interaction at nanoscale. *Nature Communications* **6**, 7359 (2015)

14. Greiner, C., Felts, J., Dai, Z., King, W. & Carpick, R. Controlling nanoscale friction through the competition between capillary adsorption and thermally activated sliding. *ACS Nano* **6**, pp. 4305-4313 (2012)
15. Chau, A., Rignier, S., Delchambre, A. & Lambert, P. Three-dimensional model for capillary nanobridges and capillary forces. *Modelling and Simulation in Materials Science and Engineering* **15**, pp. 305-317 (2007)
16. Kim, S. *et al.* Effects of Humidity on the Friction Coefficient of Diamond-Like Carbon (DLC) Coating. *Journal of Korean Physical Society* **54**, pp. 2212-2218 (2009)
17. Marino, M. *et al.* Understanding Run-In Behavior of Diamond-Like Carbon Friction and Preventing Diamond-Like Carbon Wear in Humid Air. *Langmuir* **27**, pp. 12702-12708 (2011)
18. Erdemir, A. & Donnet, C. Tribology of diamond-like carbon films: recent progress and future prospects. *J Phys D Appl Phys* **39**, pp. 311-327 (2006)
19. Arcifa, A., Rossi, A., Espinosa-Marzal, R. & Spencer, N. Influence of Environmental Humidity on the Wear and Friction of a Silica/Silicon Tribopair Lubricated with a Hydrophilic Ionic Liquid. *ACS Applied Materials & Interfaces* **8**, pp. 2961-2973 (2016)
20. Rhee, T. H., Shin, M. W. & Jang. Effects of humidity and substrate hydrophilicity on nanoscale friction. *Tribology International* **94**, pp. 234-239 (2016)
21. Sirghi, L. Effect of capillary-condensed water on the dynamic friction force at nanoasperity contacts. *Applied Physics Letters* **82**, 3755 (2003)
22. Fogden, A. & White, L.R. Contact elasticity in the precense of capillary condensation. *Jounal of Colloidal and Interface Science* **138**, pp. 414-430 (1990)
23. Gee, M., McGuiggan, P., Israelachvili, J. & Homola, A. Liquid to solidlike transitions of molecularly thin films under shear. *The Journal of Chemical Physics* **93**, 1895 (1990)
24. Jinesh, K.B. & Frenken, J.W.M. Experimental Evidence for Ice Formation at Room Temperature. *Physical Review Letters* **101**, 036101 (2008)
25. Jinesh, K.B. & Frenken, J.W.M. Capillary Condensation in Atomic Scale Friction: How Water Acts like a Glue. *Physical Review Letters* **96**, 166103 (2006)

26. Grill, A. Diamond-like carbon: state of the art. *Diamond and Related Materials* **8**, pp. 428-434 (1999)
27. Erdemir, A. The role of hydrogen in tribological properties of diamond-like carbon films. *Surf Coatings Technology* **146**, pp. 292-297 (2001)
28. Andersson, J. *et al*. Friction of diamond-like carbon films in different atmospheres. *Wear* **254**, pp. 1070-1075 (2003)
29. McFarlane, J.S. & Tabor, D. Relation between friction and adhesion. *Proceedings of The Royal Society A*, pp. 244-235 (1950)
30. Yoshizawa, H., Chen, Y. & Israelachvili, J. Fundamental mechanisms of interfacial friction. 1. Relation between adhesion and friction. *The Journal of Physical Chemistry* **97**, pp. 4128-4140 (1993)
31. Cross, R. Increase in friction force with sliding speed. *American Journal of Physics* **73**, 812 (2005)
32. Braun, O. & Peyrard, M. Dependence of kinetic friction on velocity: Master equation approach. *Physical Review E* **83**, 046129 (2011)
33. Liu, H., Ahmed, I.-U. & Scherge, M. Microtribological properties of silicon and silicon coated with diamond like carbon, octadecyltrichlorosilane and stearic acid cadmium salt films: A comparative study. *Thin Solid Films* **381**, pp. 135-142 (2001)
34. Opitz, A. *et al*. Nanofriction mechanisms derived from the dependence of friction on load and sliding velocity from air to UHV on hydrophilic silicon. *arXiv* (2005) doi:10.1007/s11249-005-8550-1
35. Chen, J., Ratera, I., Park, J. & Salmeron, M. Velocity Dependence of Friction and Hydrogen Bonding Effects. *Physical Review Letters* **96**, 236102 (2006)
36. Schirmeisen, A. *et al*. Temperature dependence of point contact friction on silicon. *Applied Physics Letters* **88**, 123108 (2006)
37. Landes, F.P. Introduction to Friction. Springer (2016)
38. Bo, L.C. & Pavelescu, D. The friction-speed relation and its influence on the critical velocity of stick-slip motion. *Wear* **82**, pp. 277-289 (1982)
39. Antoniou, S.S. *et al*.The friction-speed relation from stick-slip data. *Wear* **36**, pp. 235-254 (1976)
40. Persson, B.N.J. Theory of friction: Stress domains, relaxation, and creep. *Physical Review B Condensed Matter* **51**, 13568 (1995)

41. Zwörner, H. *et al*. The velocity dependence of frictional forces in point-contact friction. *Appl Phys Mater Sci Process* **66** (1998)
42. Braun, O.M. & Röder, J. Transition from Stick-Slip to Smooth Sliding: An Earthquakelike Model. *Physical Review Letters* **88**, 096102 (2002)
43. Bureau, L. *et al*. Low-velocity friction between macroscopic solids. C.R. Academy of Science Paris **2**, pp. 699-707 (2001)
44. Rozman, M.G. *et al*. Atomic Scale Friction and Different Phases of Motion of Embedded Molecular Systems. *The Journal of Physical Chemisctry B*, pp. 7924-7930 (1998)
45. Baumberger, T. *et al*. Physical analysis of the state- and rate-dependent friction law. II. Dynamic friction. *Phys Rev B* **60**, pp. 3928-3939 (1999)
46. Filippov, A.E., Klafter, J. & Urbakh, M. Friction through Dynamical Formation and Rupture of Molecular Bonds. *Physical Review Letters* **92**, 135503 (2004)
47. Baumberger, T. & Caroli, C. Solid friction from stick slip down to pinning and aging. *Advances in Physics* **55**, , pp. 279-348 (2008)
48. Briscoe, W. *et al.* Boundary lubrication under water. *Nature* **444,** pp. 191–194 (2006)
49. Kumar, D. *et al*. Super low to high friction of turbostratic graphite under various atmospheric test conditions. *Tribology International* **44**, pp. 1969-1978 (2011)
50. Bhowmick, S., Banerji, A. & Alpas, A. Role of humidity in reducing sliding friction of multilayered graphene. *Carbon* **87**, pp. 374-373 (2015)
51. Konca, C. *et al*. Effect of test atmosphere on the tribological behaviour of the non-hydrogenated diamond-like carbon coatings against 319 aluminum alloy and tungsten carbide. *Surface and Coatings Technology* **200**, pp. 1783-1791 (2005)
52. Ni, W. *et al*. Tribological behavior of diamond-like-carbon (DLC) coatings against aluminum alloys at elevated temperatures. *Surf Coatings Technology* **201**, pp. 3229-3234 (2006)
53. Barel, I. & Urbakh, M. Multibond Dynamics of Nanoscale Friction: The Role of Temperature. *Physical Review Letters* **104**, 066104 (2010)

54. Kalin, M. & Vizintin, J. A comparison of the tribological behaviour of steel/steel, steel/DLC and DLC/DLC contacts when lubricated with mineral and biogradable oils. *Wear* **261**, pp. 22-31(2006)
55. Bocquet L. *et al*. Moisture-induced ageing in granular media and the kinetics of capillary condensation. *Nature* **396**, pp. 735-737 (1998)
56. Gnecco E. *et al.* Velocity Dependence of Atomic Friction. *Physical Review Letters* **84**, pp. 1172-1175 (2000)
57. Sharma, N. *et al*. Velocity dependence of coefficient of friction of diamond like carbon coatings. *Solid State Physics* **1447**, pp. 651-652 (2012)
58. Li, H. *et al.* Humidity dependence on the friction and wear behavior of diamond-like carbon film in air and nitrogen environments. *Diamond and Related Materials* **15**, pp. 1585-1592 (2006)
59. Donnet, C. Recent progress on the tribology of doped diamond-like and carbon alloy coatings: a review. *Surface and Coatings Technology* **100**, pp. 180-186 (1998)
60. Shimizu, T., Kakegawa, T. & Yang, M. Micro-texturing of DLC Thin Film Coatings and its Tribological Performance Under Dry Sliding Friction for Microforming Operation. *Procedia Engineering* **81**, pp. 1884-1889 (2014)
61. Savage, R.H. & Schaefer, D. Vapor Lubrication of Graphite Sliding Contacts. *Journal of Applied Physics* **27**, 136 (1956)
62. Jiang, J., Zhang, S. & Arnell, R. D. The effect of relative humidity on wear of a diamond-like carbon coating. *Surface and Coatings Technology* **167**, pp. 221-225 (2003)
63. Hauert, R. An overview on the tribological behavior of diamond-like carbon in technical and medical applications. *Tribology International* **37**, pp. 991-1003 (2004)
64. Voevodin, A.A. *et al*. Mechanical and tribological properties of diamond-like carbon coatings prepared by pulsed laser deposition. *Surface and Coatings Technology* **76**, pp. 534-539 (1995)
65. Torun, B. *et al*. Study of water adsorption and capillary bridge formation for SiO_2 nanoparticle layers by means of a combined in situ FT-IR reflection spectroscopy and QCM-D set-up. *Physical Chemistry Chemical Physics* **16**, pp. 7377-7384 (2014)

66. Greiner, C., Felts, J., Dai, Z., King, W. & Carpick, R. Local Nanoscale Heating Modulates Single-Asperity Friction. *Nano Letters* **10**, 4640-5 (2010)
67. Sirghi, L. Transport Mechanisms in Capillary Condensation of Water at a Single-Asperity Nanoscopic Contact. *Langmuir* **28**, pp. 2558-2566 (2012)
68. Restagno, F. *et al*. Thermally activated dynamics of capillary condensation. *Journal of Physics: Condensed Matter* **12**, pp. 419-424 (2000)
69. Iwamatsu, M. & Horii, K. Capillary Condensation and Adhesion of Two Wetter Surfaces. *Journal of Colloid and Interface Science* **182**, pp. 400-406 (1996)
70. Reiss, H. & Koper, G.J.M The Kelvin Relation: Stability, Fluctuation, and Factors Involved in Measurement. *Journal Physical Chemistry* **99**, pp. 7837-7844 (1995)
71. Greiner, C., Felts, J., Dai, Z., King, W. & Carpick, R. Temperature Dependence of Nanoscale Friction Investigated with Thermal AFM Probes. *MRS Proceedings* **1226** (2009)
72. Krylov, S. & Frenken, J.W.M. Thermal contact delocalization in atomic scale friction: a multitude of friction regimes. *New Journal of Physics* **9**, 398 (2007)
73. Schwarz, U. & Hölscher, H. Exploring and Explaining Friction with the Prandtl–Tomlinson Model. *ACS Nano* **10**, pp. 38-41 (2016)
74. Zhao, X. *et al*. Transition from Thermal to Athermal Friction under Cryogenic Conditions. *Physical Review Letters* **102**, 186102 (2009)
75. Heimberg, J. Superlow friction behavior of diamond-like carbon coatings: Time and speed effects. *Applied Physics Letters* **78**, 2449 (2001)
76. Si-mat.com/silicon-wafers.html Visited on 05 April 2017
77. Popova, E. & Popov, V.L. The research works of Coulomb and Amontons and generalized laws of friction. *Friction* **3**, pp. 183-190 (2015)
78. https://www.vaisala.com/ Visited on 09 April 2017
79. De Barros Bouchet, M.-I. *et al*. Friction of diamond in the presence of water vapor and hydrogen gas. Coupling gas-phase lubrication and first-principles studies. *Journal of Physical Chemistry C*, **116**, pp. 6966-6972 (2012)
80. Levita, G., Restuccia, P. & Righi, M.C. Graphene and MoS_2 interacting with water: A comparison by ab initio calculations. *Carbon* **107**, pp. 878-884 (2016)

81. Kim, S. *et al.* Effects of Humidity on the Friction Coefficient of Diamond-Like Carbon (DLC) Coating. *Journal of Korean Physical Society* **54**, pp. 2212-2218 (2009)
82. Erdemir, A. & Eryilmaz, O. Achieving superlubricity in DLC films by controlling bulk, surface, and tribochemistry. *Friction* **2**, pp. 140-155 (2014)
83. Scharf, T.W. & Singer, I.L. Quantification of the Thickness of Carbon Transfer Films Using Raman Tribometry. *Tribology Letters* **14**,pp. 137-145 (2003)
84. Brennan, J. *et al*. Adsorption of Water in Activated Carbons: Effects of Pore Blocking and Connectivity. *Langmuir* **18**, pp. 5438-5447 (2002)